

# Averaging the spectral shapes

Piotr Lubinski<sup>?</sup>

N. Copernicus Astronomical Center, Bartycka 18, 00-716 Warsaw, Poland

Accepted ... Received ...; in original form ...

## ABSTRACT

The methods of obtaining the average spectral shape in a low statistics regime are presented. Different approaches to averaging are extensively tested with simulated spectra, based on the ASCA responses. The issue of binning up the spectrum before fitting is discussed together with the choice of statistic used to model the spectral shape. The best results are obtained with methods in which input data are represented by probability density functions. Application of weights, representing the coverage between the input and output bins, slightly improves the resolution of averaging.

**Key words:** spectral shape { Fe K line.

## 1 INTRODUCTION

Spectral information obtained from X-ray astronomy instruments is usually the result of a compromise between the aim of achieving the best possible energy/spatial resolution and the purpose of collecting a large number of photons. In consequence, there will be always some class of objects which are too faint, with spectra which cannot be studied with all desired particulars. The problem of a lack of statistics can be solved to some extent by averaging a number of weak spectra, but this implies examination of rather common properties. Nevertheless, since spectra can be grouped into subsamples according to some better established quantities such as the continuum slope, flux, hardness ratio, etc., this method may be quite powerful for studying various correlations.

A clear distinction should be made between the average spectrum and the average spectral shape. The former is simply the average flux and the result is dominated by the brightest objects or states (in the case of average for a single object). The latter is the average of a relative quantity, spectral shape, usually defined as the ratio between data and a simple continuum model, common for all studied objects. Such a proportion is often employed to bring some discrete features into prominence | a well known example is e.g. 1 of Tanaka et al. (1995) where the redshifted iron K line profile, observed for MCG-6-30-15, was shown. The shape defined as above is customarily used only for illustrative purposes, e.g., Reynolds (1997) and Reeves (2003). However, the average shape can be constructed and studied in a quantitative way, as was done for the spectra of Sey1 nuclei observed by ASCA (Nandra et al. 1997a,b). A similar investigation was performed later for a larger sample of Sey1 ASCA observations (Lubinski & Zdziarski 2001), where average shape

spectra were obtained for subsamples grouped according to the continuum slope. The 'average shape spectrum' is defined as the average data to continuum model ratio (i.e., the average shape), multiplied by the average continuum model (model with the average parameters calculated with a standard weighted mean).

The average profiles of the iron K line presented in Nandra et al. (1997a) and in Lubinski & Zdziarski (2001) are clearly distinct. This difference was ascribed partially to the change in calibration of ASCA SIS detectors done after 1997 and partially to a different approach to averaging. However, the first explanation was later questioned and the whole difference was assigned to the dissimilar averaging procedure (Yaqoob et al. 2002). The issue of changed calibration will be discussed elsewhere; here we want to consider the problem of correct averaging. An additional motivation comes from the fact that it seems promising to apply similar averaging procedures to the data from other missions, such as Chandra, XMM-Newton, and, in future, Astro-E. Therefore, it is important to have at one's disposal a verified method, exploiting all available information in the most efficient and accurate way.

In the following sections we discuss three basic aspects of spectral shape averaging: bin weights, prebinning and the character of the data. The first is the way in which the information on the relative positions of the input and output bins is taken into account. Prebinning means here the summing of counts from a single input spectrum over the span of the output bin. Finally, the Poisson character of the data is important for low numbers of counts where the standard weighted average, which assumes a symmetric, Gaussian probability density distribution, cannot be used. These aspects are connected | for example, prebinning leads to the loss of some information on the data distribution in input bins, but, on the other hand, increases the number of counts. Various approaches to these basic issues can be combined to construct

<sup>?</sup> E-mail: piotr@cam.k.edu.pl

different averaging methods; our aim is to test them through extensive tests performed on simulated data.

## 2 AVERAGING METHOD

### 2.1 Rebinning

By definition, the average value of a function  $f(e)$  over the range of its argument,  $(e_i; e_{i+1})$ , is equal to the ratio of this function integral over this range to the length of this range,

$$h_{i,j} = \frac{\int_{e_i}^{e_{i+1}} f(e) de}{e_{i+1} - e_i} = \frac{\int_{e_i}^{e_{i+1}} f(e) de}{e_i} \quad (1)$$

Here and after we use the following convention: angle brackets  $h_i$  denote the average over some range of the function argument, i.e., rebinned value, without weights associated with the accuracy of the averaged quantity. Any average, for a single spectrum or for many spectra, weighted by the accuracy weights is indicated by a dash over the symbol. Subscripts  $i; j; k$  are used for input data, spectra and output data, respectively. To distinguish if the input data are summed or averaged for a single spectrum or for all spectra, we will use different upper summation limits,  $n_{kj}$  for a single,  $j$ -th spectrum and  $n_k$  for all spectra. The output data for an individual spectrum will be denoted by an additional index  $j$ . Finally, the number of averaged spectra is equal to  $n_s$ .

Assume that we know the averages of a certain energy function for some initial distribution of energy ranges  $e_i$  and we want to determine averages for another set of energy ranges  $E_k$ . This is rebinning: for a given spectrum, values in some bins are converted to values in bins occupying different ranges. The idea of rebinning is illustrated in Fig. 1. In general, the output bin  $k$ , with boundaries  $(E_k; E_{k+1})$ , for a spectrum numbered with  $j$  expands over  $n_{kj}$  input bins (with lower limits  $e_0; e_1; \dots; e_{n_{kj}-1}$  and upper limits  $e_1; e_2; \dots; e_{n_{kj}}$ ). The first and the last input bins can lie partially outside the output bin. Input data are discrete, we know only the average of the unknown function  $f(e)$  measured by the detector over the  $i$ -th bin, its value  $h_{i,j}$  is attributed to the centre of the bin. Using the approximation that  $f(e)$  is constant within an input bin and introducing bin weights  $b_i$  we obtain the formula for the rebinned value  $h_{k,j}$  in the form

$$h_{k,j} = \sum_{i=1}^{n_{kj}} b_i h_{i,j} \quad (2)$$

$$b_i = \begin{cases} \frac{e_1 - E_k}{E_k - E_{k-1}}; & \text{partial overlap, left boundary;} \\ \frac{e_i - E_k}{E_k - E_{k-1}}; & \text{full overlap, inside output bin;} \\ \frac{E_{k+1} - e_{n_{kj}}}{E_{k+1} - E_k}; & \text{partial overlap, right boundary;} \\ 1; & \text{input bin covers output bin,} \end{cases} \quad (3)$$

and

$$b_i = 1: \quad (4)$$

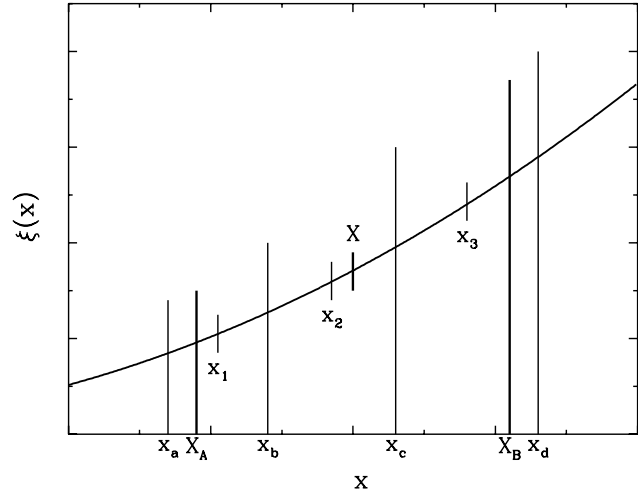


Figure 1. Idea of rebinning of function over some range of its argument. The average for segment  $(E_k; E_{k+1})$  is determined using the known averages for segments  $(e_0; e_1)$ ,  $(e_1; e_2)$ , ...,  $(e_{n_{kj}-1}; e_{n_{kj}})$ .

Defining  $b_i$  as the width of the overlap between input bin  $i$  and output bin  $k$ , the weights  $b_i$  may be simply expressed as  $b_i = E_k$ .

Boundary input bins, with the same value of weight  $b_i$ , can occupy quite different ranges outside the output bin. Hence, they can represent different information on the averaged function, integrated over a different range of argument. To take this fact into account one can apply another bin weight, inversely proportional to the input bin width, equal to  $1/e_i$  or, better, to  $b_i = e_i$ .

Figure 2 shows an example of averaging with and without bin weights. The averaged function  $f(E)$  is a constant plus Gaussian peak plus an edge, modelled by a negative half-Gaussian. The widths of Gaussians were set to 0.02 keV and 0.1 keV for peak and edge, respectively. This function was integrated over 0.01 keV bins to obtain the reference shape after using the instrument with 0.01 keV energy resolution. The function was then integrated 200 times for random binning patterns, with bin widths  $e_i$  taken from some interval. The resulting 'spectra' were rebinned in four different ways (with bin weights listed in Fig. 2) to 0.01 keV output bins and the results were compared with the reference shape. The whole procedure was repeated for different ranges of input bin widths. When the input bins  $e_i$  are much broader than 0.01 keV the resulting averages with and without bin weights are indistinguishable. For input bin widths comparable to or less than 0.01 keV, the differences in results correlate with decreasing input bin width. Procedures with bin weights clearly better reproduce the sharp features of the averaged function than the simple arithmetic average, the best of these is the weight in the form  $b_i^2 = e_i$  but the differences are rather small.

Bin weights play a role similar to approximating the shape of the rebinned function with a polynomial spline. However, for poor quality data they are safer than any iterative spline procedure, because the latter method may amplify some spurious spectral features during consecutive iterations. Therefore, since we have to work with low statistics

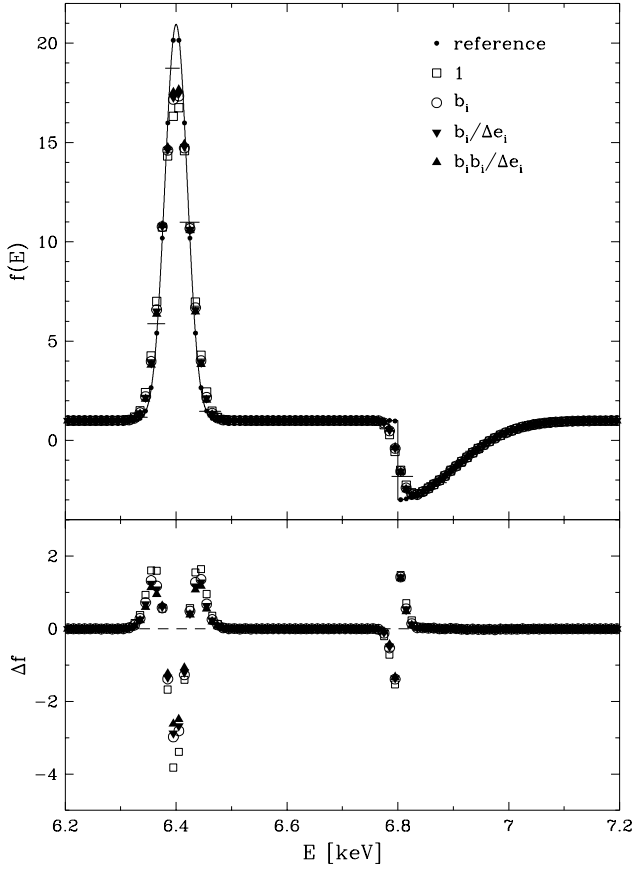


Figure 2. Upper panel: Averaging of function with and without bin weights. Solid line shows the averaged function  $f(E)$ , reference shape (dots) is the result of integrating this function over 0.01 keV bins. Averaged data are obtained by integrating  $f(E)$  with random bin widths taken from 0.01–0.02 keV range (an example of these bins is shown with the horizontal lines). The average shapes were calculated for 200 input data sets, with output bin widths equal to 0.01 keV and using 4 different bin weights. Lower panel shows the differences between the results of averaging and the reference shape.

data and since the energy resolution of ASCA SIS detectors is not so high, the discrete spectral features can be well traced by bin weights alone, without using an additional spline approximation. Moreover, any more complex spline procedure applied to a small set of weak spectra may lead to a quite accidental approximation of the local spectral shape. On the contrary, bin weight values are well defined, do not depend on the averaged function value and control the relevance of information given by the input bin, comparing simply input and output bin locations.

## 2.2 Prebinning

The quantity which we intend to average is the ratio of measured and modelled fluxes. Since the flux is proportional to the number of counts we can utilize the fact that the number of counts measured for a broader bin is equal to the sum of counts collected for narrower bins constituting this broad bin. Then, instead of averaging input flux ratios for a given output bin, we can directly determine data and model fluxes

for that bin. The measured flux,  $hfi_{kj}$ , is equal to the sum of all net counts  $D_i$ , divided by appropriate detector area  $A_i$ , and normalized with the observation time,  $T$ , and output bin width,  $E_k$ ,

$$hfi_{kj} = \frac{\sum_{i=1}^{n_{kj}} g_i D_i A_i}{T E_k}; \quad (5)$$

where weights  $g_i = 1/e_i$  ( $= b_i E_k = e_i$ ) are introduced for boundary input bins, only partially overlapping with the output bin.

In practice, there is no simple method of performing spectral fitting with arbitrary energy bins, i.e., with energy bins adjusted to cover the output bins. This is due to the fact that the instrumental response function is defined as a matrix for a fixed set of energy bins. Therefore, it is necessary to perform prebinning with model counts determined for input channels instead of fitting them for output bins. The modelled flux,  $hfi_{kj}^m$ , is expressed through the model net counts,  $M_i$ ,

$$hfi_{kj}^m = \frac{\sum_{i=1}^{n_{kj}} g_i M_i A_i}{T E_k}; \quad (6)$$

The numerator in (5) can be replaced by  $\sum_{i=1}^{n_{kj}} g_i D_i A_k$ , where the area  $A_k$  represents the effective detector efficiency for bin  $k$ . After similar replacement in (6), the ratio of the data and model fluxes for output bin  $k$  is equal to

$$hri_{kj} = \frac{\sum_{i=1}^{n_{kj}} g_i D_i}{\sum_{i=1}^{n_{kj}} g_i M_i}; \quad (7)$$

The procedure with prebinning is simpler than that based on averaging all input ratios  $hri_i$  ( $= D_i/M_i$ ); after prebinning one has only to average ratios  $hri_{kj}$  obtained for the output bins from various spectra. Nevertheless, there is one disadvantage: the information included in the input ratios  $hri_i$  is lost. The issue of how this affects the results by reducing the resolution will be discussed later, in Sec. 5.

## 2.3 Accuracy weights

The initial ratios  $hri_i$  are measured with some finite accuracy and this should be taken into account in averaging. For the set of  $n_{ks}$  independent ratios, described by the probability density functions  $p_i(r)$ , the mean value (centre of gravity) is given by the integral

$$\bar{r}_k = \frac{\int_{-R_1}^{R_1} r p_k(r) dr}{\int_{-1}^1 p_k(r) dr}; \quad (8)$$

where the joint density function  $p_k(r)$  is equal to the product of partial densities

$$p_k(r) = \prod_{i=1}^{n_{ks}} p_i(r); \quad (9)$$

The standard deviation for  $\bar{r}_k$ ,  $\sigma_{r_k}$ , is calculated from the variance definition

$$\sigma_{r_k}^2 = \frac{\int_{-R_1}^{R_1} (r - \bar{r}_k)^2 p_k(r) dr}{\int_{-1}^1 p_k(r) dr}; \quad (10)$$

## 2.4 Standard average

In the case where the densities  $p_i(r)$  have Gaussian shape, centered at  $hri_i$  and with width parameters  $b_i$ , one obtains from (8) and (10) the standard formula for the weighted mean and its uncertainty

$$\bar{r}_k = \frac{\sum_{i=1}^{n_{ks}} w_i hri_i}{\sum_{i=1}^{n_{ks}} w_i}; \quad \bar{r}_k = \frac{1}{\sum_{i=1}^{n_{ks}} w_i}; \quad (11)$$

where weights  $w_i$  are equal to  $1/(b_i)^2$ .

The above formula can be applied to ratios obtained from larger numbers of counts, when the Poisson probability function associated with the data can be approximated by a Gaussian function. In such a case, the unknown uncertainty of the true number of counts can be approximated by the square root of the measured number of counts. Then, the ratio uncertainty  $hri_i$  is equal to  $\sqrt{g_i N_i + g_i B_i} = g_i M_i$ , where  $N_i$  denotes the source (net effect + background) number of counts and  $B_i$  is the background number of counts. Weights  $g_i$  modify these numbers for an input bin lying on the boundary of the output bin. In Appendix A it is shown that for relative quantities such as flux, the accuracy weights  $w_i$  to some extent play a role similar to the bin weights.

Obviously, the condition of large number of counts can be more easily fulfilled in the case of prebinned data, when the output bins are broader than the input ones. The uncertainty of ratio  $hri_{kj}$ , given by equation (7), is then approximated by

$$hri_{kj} = \frac{\sum_{i=1}^{n_{kj}} g_i N_i + \sum_{i=1}^{n_{kj}} g_i B_i}{\sum_{i=1}^{n_{kj}} g_i M_i}; \quad (12)$$

The ratio  $\bar{r}_k$  and its uncertainty  $\bar{r}_k$  for prebinned data, averaged over all spectra, is calculated from (11), with  $hri_i$  replaced by  $hri_{kj}$ , weights  $w_{kj}$  equal to  $1/(hri_{kj})^2$  and summation going from  $j = 1$  to  $j = n_s$ .

## 2.5 Combined weights

According to the results of Sec. 2.1, the accuracy weighted average for input ratios  $hri_i$  should be modified to incorporate bin weights. Application of another type of weight, such as bin weights  $b_i$ , can be realized via broadening of the probability density distributions associated with the data by raising them to a power equal (or proportional) to this additional weight. It should be stressed that this procedure is used only to change the relative widths of these distributions, by taking into account the overlap between given input bin  $i$  and output bin  $k$ . There is, then, some arbitrariness in defining the broadening power index. In tests with simulated spectra, we found that the change of  $b_i$  to  $b_i = 10$  or  $10b_i$  affects only the fifth digit in the result of averaging. Nevertheless, any broadening of the initial distributions leads to a change of the width of resulting distribution, hence affects the error of  $\bar{r}_k$ . For narrow input bins ( $b_i \ll 1$ ) the normal distribution can be quite broad and its dispersion should be renormalized, since bin weights are used only to refine the calculation of the average, and should not change the accuracy of the input  $hri_i$  values. To avoid absolute narrowing of any of initial distributions the renormalization is done by replacing  $b_i$  in the above equation by  $\hat{b}_i = b_i \max(b_i)$ . This leads to only slightly broader distributions than those obtained without bin weights.

The combined weights for the standard average are equal to  $\hat{b}_i w_i$ , since the width of broadened Gaussian is equal to  $1/\hat{b}_i$ . However, the combined weighted average and its propagated error, calculated from (11), can be expressed using weights  $b_i$  directly, due to the fact that the normalizing factors  $1/\max(b_i)$  in numerator and denominator cancel out

$$\bar{r}_k = \frac{\sum_{i=1}^{n_{ks}} b_i w_i r_i}{\sum_{i=1}^{n_{ks}} b_i w_i}; \quad \bar{r}_k = \frac{\sum_{i=1}^{n_{ks}} b_i^2 w_i}{\sum_{i=1}^{n_{ks}} b_i w_i}; \quad (13)$$

The above formulae were used to obtain the average spectral shape for Sy1 active nuclei observed by ASCA (Lubinski & Zdziarski 2001). However, some correction should be made: weights  $w_i$  for border input bins should be decreased by a factor equal to weight  $g_i$ , since the  $hri_i$  error is increased by  $1/g_i$  due to only a partial share of input bin flux in the flux of the output bin. In consequence, we obtain

$$\bar{r}_k = \frac{\sum_{i=1}^{n_{ks}} b_i g_i w_i r_i}{\sum_{i=1}^{n_{ks}} b_i g_i w_i}; \quad \bar{r}_{ks} = \frac{\sum_{i=1}^{n_{ks}} b_i^2 g_i w_i}{\sum_{i=1}^{n_{ks}} b_i g_i w_i}; \quad (14)$$

As discussed in Sec. 5.2, the above correction affects mainly the ratio errors, leaving the ratio values almost unchanged.

## 2.6 Average for Poisson data

The formula given by (11) is derived from the definition of the mean (Eq. 8) for quantities described by the probability density function in Gaussian form. However, the numbers of counts collected in a single channel by SIS instruments of ASCA for weak sources such as AGNs are very small | above 7 keV these numbers are often equal to 1 or 0. Therefore, equation (11) cannot be used for a low number of counts, where the Poisson distribution differs substantially from the Gaussian one. Moreover, in this situation the unknown uncertainty of the true number of counts cannot be approximated by the square root of the measured number of counts.

Individual densities in the counts space,  $p_i()$ , including the case of border input bins with numbers of counts modified by weights  $g_i$ , can be expressed as Poisson functions of unknown mean  $\mu$ , with observed  $g_i N_i$  source counts and  $g_i B_i$  background counts as parameters

$$p_i() = C_i \frac{e^{-(g_i N_i + g_i B_i)} (g_i N_i + g_i B_i)^{g_i N_i}}{(g_i N_i + 1)!}; \quad (15)$$

where constant  $C_i$  ensures proper normalization of the probability function. The above formula has the form of a Poisson distribution, however, here the problem is inverted | we are interested in a function of continuous argument for given numbers of observed counts.

Because numbers of counts modified by weights  $g_i$  are not necessarily the integer numbers, the standard factorial present in the Poisson distribution definition, in Eq. (15) is replaced by the complete gamma function  $\Gamma(g_i N_i + 1)$ . For the same reason we cannot give an analytical expression for the normalizing factor, (cf. Eq. (B3) in Appendix B), because for non-integer  $g_i N_i$  the expansion of  $(g_i N_i + g_i B_i)^{g_i N_i}$  binomial is not finite, and value of  $C_i$  has to be computed by numerical integration.

The formula (15) is based on the assumption that the background number of counts is known precisely. Evidently, in a real situation we do not know the true background rate. However, as will be shown in Sec. 5, this assumption is sufficient to give proper averaging results. Our main goal is to describe the data probability distribution in a way more valid than a Gaussian distribution, and Eq. (15) leads to a satisfactory result.

Nevertheless, in Appendix B we present two solutions to the problem of the unknown background which we have found in literature. As can be expected, these procedures lead to a more diffuse distribution than that given by (15), especially with a broadened left tail when the observed background number of counts is close to zero. We have tried to include these methods in the averaging code, but, because of some problems with the implementation of these methods in current versions of popular spectral fitting codes (see next Section) we cannot model the continuum in a corresponding way. Therefore, the treatment of data in averaging and in continuum modelling cannot be consistent, and, in consequence, the data/model ratios will diverge.

Direct calculations based on Eq. (15) are impractical for larger values of  $g_i N_i$ . Therefore the function  $p_i(\lambda)$  is calculated using the algorithm invented for computing the binomial distribution (Loader 2000). Computation, except for the trivial case when  $g_i B_i = 1$ , reduces to calculating the exponent of some function  $f_i(\lambda)$ , depending on  $g_i$  and  $B_i$ , normalized with some factor  $\alpha_i$  depending on  $N_i$ ,  $B_i$  and  $g_i$ . Then the probability density can be given in the form

$$p_i(\lambda) = \frac{e^{-f_i(\lambda)}}{\alpha_i (g_i N_i; g_i B_i)}; \quad (16)$$

Turning to ratios, we take into account the modelled number of counts,  $g_i M_i$ , and the averaging reduces to determining the mean of the joint density distribution function

$$p_k(r) = \prod_{i=1}^{K_s} C_i e^{g_i(r)}; \quad (17)$$

where the function  $e^{g_i}$  is equal to  $f_i$  with an argument scaled by the factor  $1 = g_i M_i$  and the normalizing factors  $C_i$  are functions of  $N_i; B_i, M_i$  and  $g_i$ .

In the case of prebinned data, for a spectrum numbered with  $j$  we have function  $f_{kj}$  and factorial  $C_{kj}$  depending on the summed counts  $\sum_{i=1}^{n_{kj}} g_i N_i$ ,  $\sum_{i=1}^{n_{kj}} g_i B_i$  and  $\sum_{i=1}^{n_{kj}} g_i M_i$ , and the joint density distribution function is calculated for  $n_s$  spectra

$$p_k(r) = \prod_{j=1}^{N_s} C_{kj} e^{g_{kj}(r)}; \quad (18)$$

At last, when bin weights  $\hat{b}_i$  are taken into account for data without prebinning, the formula for the joint probability density functions has the form

$$p_k(r) = \prod_{i=1}^{K_s} C_i e^{g_i(r)} \hat{b}_i; \quad (19)$$

There is no computer on Earth able to directly multiply many very small numbers, which are unavoidable for a broad range of ratio values, especially when  $n_{ks}$  is of the order of thousand and the multiplied distributions are narrow. Thus it is necessary to replace  $p_k(r)$  with its logarithm

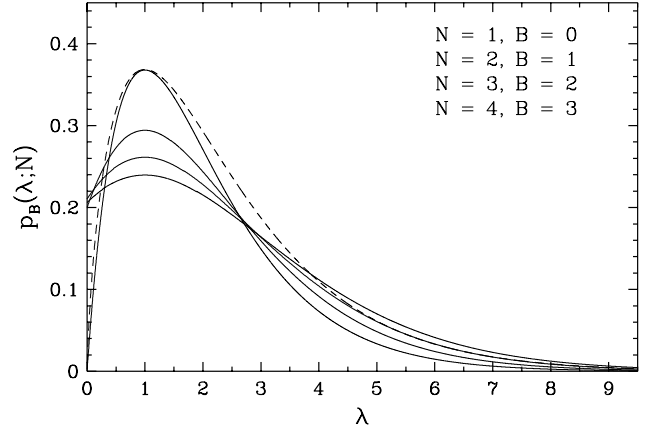


Figure 3. Four probability functions (Eq. (15)) for net counts  $D = 1$  and background counts  $B$  equal to 0, 1, 2, 3 (from top). For  $N = 1$  the example of broadening of the probability density function by the bin weight = 0.75 is shown with a dashed line.

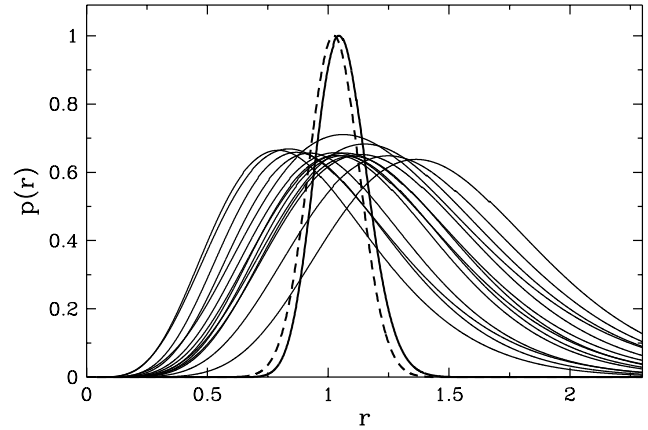


Figure 4. Example of the joint probability distribution applied to determine the mean ratio. Thin lines show the Poisson probability functions representing the averaged input ratios, thick solid line shows their product distribution, normalized to have a maximum equal to 1. Dashed line illustrates the product distribution obtained when the input data are given by the Gaussian probability functions.

$$\begin{aligned} \log p_k(r) &= \log \prod_{i=1}^{K_s} C_i e^{g_i(r)} \hat{b}_i = \sum_{i=1}^{K_s} \log C_i + \sum_{i=1}^{K_s} g_i(r) \hat{b}_i \\ &= \sum_{i=1}^{K_s} \hat{b}_i g_i(r) + \sum_{i=1}^{K_s} \hat{b}_i \log C_i; \end{aligned} \quad (20)$$

The second sum in the last line of the above equation can be dropped since it only corresponds to adding a constant to the density distribution function and the computed density function is

$$\log p_k(r) = \sum_{i=1}^{K_s} \hat{b}_i g_i(r); \quad (21)$$

The final average  $\bar{r}_k$  is found from equation (8) as the

mean of the exponent of the above function but with the lower integral limit equal to 0, since the number of counts (or ratio) cannot be negative. Accordingly, the accuracy of  $\bar{r}_k$  is calculated from Eq. (10).

The joint density function  $p_k(r)$  is constructed as a likelihood function in the maximum likelihood estimation method. Then, the best estimator for  $\bar{r}_k$  is the mode, for which the accuracy should be calculated using the second derivative of  $p_k(r)$ . The computation of mode for density function given by Eq. (8) is simple but numerical determination of its second derivative and then its expectation value to assign the accuracy to  $\bar{r}_k$  for many input bins may significantly increase the computation time. Therefore, because the normal distribution functions are usually quite symmetric, especially for a larger number of averaged spectra, the mode and its error were replaced here by the mean and standard deviation. As it was tested, even for an extreme case of a single, weak spectrum, the difference between mode and mean of  $p_k(r)$  does not exceed 0.5%.

### 3 CONTINUUM MODEL

Considering the issue of averaging the data/model ratios in Sec. 2.2, we have concluded that the continuum model should be fitted to the non-binned spectrum, i.e., collected with original, single SIS channels. Due to this fact, for a low number of counts we also have to treat the spectral modelling in a non-standard manner. Since the  $\chi^2$ -statistic cannot be applied during fitting, an alternative approach is needed. A fairly popular and well established solution is the C-statistic (Cash 1979). It is based on the maximum likelihood method, and has no limitation according to the number of counts. In the case of  $N_i$  source counts and  $S_i$  model counts it is defined as (Freeman, Doe & Siemiginowska 2001)

$$C = 2 \sum_{i=1}^{N_c} (S_i - N_i \ln S_i); \quad (22)$$

where  $N_c$  is the number of data channels.

The difference of two Poisson distributions is not Poisson distributed, thus the C-statistic cannot be applied to background subtracted data. Therefore in the C-statistic case the source and background spectra were fitted simultaneously. The net number of model counts  $M_i$  was determined by subtracting the appropriate numbers modelled for a given channel. In consequence, data in modelling were treated in a way consistent with averaging based on equation (15).

The C-statistic is implemented in both most popular X-ray spectra fitting codes, XSPEC (Arnaud 1996) and SHERPA (Freeman, Doe & Siemiginowska 2001). However, used within XSPEC it produced biased results: the fitted power law indices and normalizations were much larger than those assumed in the simulated model.<sup>1</sup> Therefore, in the case of non-rebinned spectra, fitting them model of continuum used to normalize observed data to obtain the spectral shape was done only with SHERPA. For comparison, we have also

binned up spectra and fitted them with a  $\chi^2$ -statistic using both XSPEC and SHERPA. All tests were performed with XSPEC, version 11.1 and SHERPA, version 2.3.

There is a Bayes statistic option in SHERPA, which corresponds to the method derived by Loredo (1992). We have tested also this approach during spectral fitting, unfortunately the results were similar to the results obtained with the C-statistic and XSPEC: the fitted power law was much steeper than the model assumed in the simulation of the spectrum. Hence, since the usage of the Bayes statistic in SHERPA seems to be somewhat uncertain and since the results obtained with C-statistic and SHERPA are quite satisfying, we do not use the Bayes approach in the tests described later.

All continuum models for the source and background spectra were fitted in the energy range (3-4.5, 7.5-10) keV, i.e., the reference continuum shape was determined in the vicinity of the Fe K line but without the line region itself. We used a power law model, assuming independent slope parameters for source and background and independent normalization for each spectrum.

### 4 TESTS

#### 4.1 Reference shape

The procedure developed for averaging the spectral shapes has to be verified, moreover, some tests of its alternatives are needed. It is obvious that such tests cannot be done for real data, as we must know the actual average shape to have a reference. For this purpose we have simulated 100 spectra for each of two SIS instruments. The reference model was similar to that obtained for the average ASCA Sy1 nuclei spectral shape (Lubinski & Zdziarski 2001). Simulations were done with responses from different periods of ASCA mission. The width of a single SIS channel was equal to 14.6 eV, since we used the BRIGHT2 data model with 1024 channels. As the starting conditions we adopted exposure times and background spectra obtained for five observations of IC 4239A, which were short, with an elapsed time of 7-18 ks. The background spectra were extracted for rather small regions with a radius of 28.5 SIS pixels. Hence, we tested a rather extreme case of low statistics to be sure that the method behaves well on the boundary of its application area.

In the upper part of Figure 5 we have shown our reference model, consisting of a broad, disc line component, a narrow, Gaussian line component and continuum in the form of power law. The parameters of the model were as follows: power law index,  $\Gamma = 1.8$ , power law normalization,  $A = 2.333 \times 10^2 \text{ keV}^{-1} \text{ cm}^{-2} \text{ s}^{-1}$ , disc line energy, 6.4 keV, inner disc radius,  $6 \text{ GM} = c^2$ , outer disc radius,  $1000 \text{ GM} = c^2$ , disc emissivity in the form  $(1 - \frac{6}{6+R}) = R^3$ , inclination,  $45^\circ$ , Gaussian line energy, 6.4 keV, Gaussian line width, 0.01 keV. The normalization of disc line and Gaussian components was adjusted to get equivalent widths equal to 130 eV and 60 eV, respectively.

Spectral shape is defined as the ratio between observed data and fitted continuum model, thus the reference model should be transformed in the same way. The reference data were simulated with a very long exposure time,  $10^9$  s, using responses of original IC 4239A spectra. Then, the contin-

<sup>1</sup> There was a bug in XSPEC, repaired in the its version 11.2.0b, after preparation of this paper. Now XSPEC used with the C-statistic produces results consistent with those obtained with SHERPA.

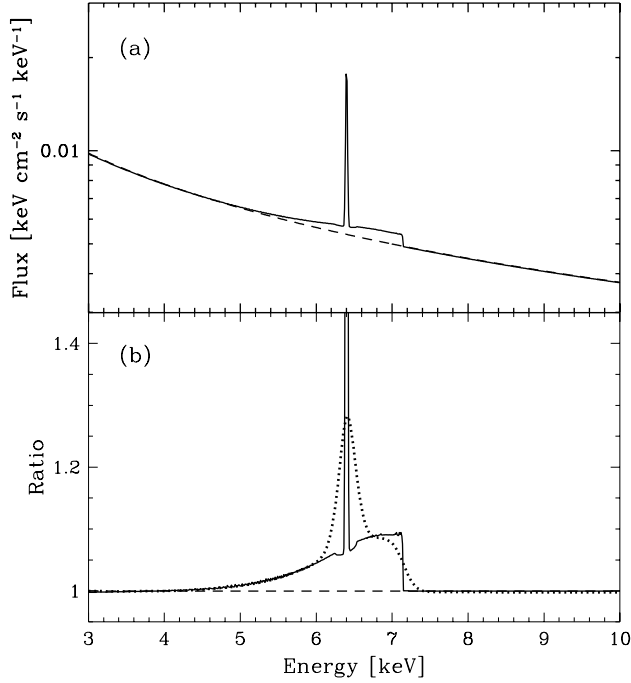


Figure 5. (a) Model function (solid line) consisting of a disc line and a Gaussian together with the power law continuum. Dashed line shows the continuum model, i.e., power law fitted outside the Fe line region, in the energy ranges 3-4.5 and 7.5-10 keV. (b) Ratio of the line and continuum model functions (solid line) compared with the data/model ratios (dots) obtained for the simulated reference spectra.

uum for the reference spectra was modelled with a power law model outside the iron line region. Resulting data/model ratios were averaged with weights equal to the original observation times, to take into account changes of SIS responses during satellite operation. These reference ratios are presented in the lower part of Fig. 5. Rebinning with finite bin width always leads to a change in the function shape, thus the results of averaging done with tested methods are compared not only with the reference ratios obtained for a single input bins, but also with the results of averaging these ratios to appropriate output bins. This reference averaging was done with our best method Ia (described below), but for such a high number of counts all procedures produce almost indistinguishable results.

#### 4.2 Tested methods

Various averaging procedures can be constructed on the basis of three elements: accuracy weights, bin weights and prebinning. We have tested some of these combinations to check their behaviour in different situations. Table 1 presents the characteristics of the tested procedures. Methods numbered with I are based on determination of the joint density function, methods II are those using the accuracy weights  $w_i$ , and method III is the arithmetic average with prebinning. Among them, method IIe uses the standard weighted average (11) applied to only those input bins, whose centres lie in the given output bin. Since this procedure is probably the

Table 1. Averaging methods tested with simulated spectra. PF denotes the probability density function. Bin weights equal to 1 mean that the input bin is taken into account only in calculating the average for the output bin containing its centre.

Method	Accuracy weights	Bin weights	Prebinning	Formula
Ia	PF	$g_i$	yes	(18)
Ib	PF	$g_i$	no	(17)
Ic	PF	$b_i g_i$	no	(19)
IIa	$w_i$	$g_i$	yes	(7,11,12)
IIb	$w_i$	$g_i$	no	(11)
IIc	$w_i$	$b_i g_i$	no	(14)
IId	$w_i$	$b_i$	no	(13)
IIe	$w_i$	1	no	(11)
III	1	$g_i$	yes	(2,7)

one most common only used, it will be termed 'standard' in the rest of the paper.

Tested methods were applied to three types of 'data/model' data. The first one was obtained for spectra with original SIS channels and the continuum model fitted with the C-statistic. The data of the second type are those from spectra binned up<sup>2</sup> firstly to gather at least 20 counts per channel, whereas continuum is modelled again with the C-statistic. The third is the case of binned up spectra and the model fitted with  $\chi^2$  statistic.

The results of the tests are presented in Figs. 6, 7, 8, the reference ratios are shown with a solid line, whereas the reference average for output bin width equal to 0.1 keV is plotted with dots. Tests were performed for different widths of output bins, here we present only results for 0.1 keV bins since this value corresponds to the ASCA SIS resolution for the iron line energy.

In order to check how the fitted continuum models reproduce the reference model, a weighted average of power law parameters was calculated for each data set. These results are presented in Table 2. Since there is still a small tail of the disc line component below 4.5 keV, the power law fitted to the reference data (simulated with long exposure) is slightly less steep ( $\Gamma = 1.798$ ) than the initial power law used in simulations ( $\Gamma = 1.8$ ). All models fitted with the C-statistic give almost correct results, whereas fitting with the  $\chi^2$  statistic leads to a clearly biased result. A similar effect was already studied by the Chandra X-ray Center staff (Freeman 2001).

Non-uniform binning up of data before fitting changes the relative influence of different parts of the spectrum on the fitted model. For a simple continuum model like power law this effect is almost negligible (cf. results from row 2 and rows 3,4 in Table 2), however, for more complex models such a procedure should be applied with some caution.

<sup>2</sup> Regarding to arithmetics, 'binning up' is a special case of prebinning, introduced in Sec. 2.2, done for the output bin covering exactly the sum of input bins. Nonetheless, there is a clear difference in applying these two procedures, the former is used before fitting the continuum model, the second uses the results of the model fitted to the initial input bins.

Table 2. Mean values of the continuum model parameters determined for various input data and fitting procedure combinations. The first row presents the results obtained for the reference data.

Binning up	Statistic	Normalization		Index	
none	both	23.28	0.01	1.798	0.001
none	C, SHERPA	23.23	0.18	1.798	0.006
biased	C, SHERPA	23.12	0.19	1.794	0.006
random	C, SHERPA	23.26	0.19	1.800	0.006
biased	$\chi^2$ , XSPEC	23.55	0.22	1.829	0.007

#### 4.3 Biased vs. unbiased binning up

The standard, initial binning up method, based on adding counts from single channels to get at least a given number of counts is biased in this sense that resulting bin widths are inversely proportional to the measured flux. Then, on average, broader input bins are more frequent for ratios below 1 than for ratios above 1. In consequence, bin weights  $b_i$  are usually smaller for ratios  $> 1$  than  $b_i$  for ratios  $< 1$  and this leads to a biased average shape. To test this effect we have prepared ‘data/model’ data with random binning, where binning up pattern for a given spectrum was taken from the other spectrum, randomly selected. In this way the binning should be non-biased, without correlation between bin widths and ratios. These spectra were fitted with C-statistic and they are the fourth type of ‘data/model’ data tested with some methods.

#### 4.4 Inhomogeneous shapes

Consider a special situation: there are two distinct classes of objects, with Fe line average shapes clearly different, and, in addition, objects of one class are much brighter than those of the second class. Then, if the spectra were taken in similar conditions (i.e., with approximately equal exposures), their weighted average will be far from the true, physical mean for these two classes. We have tested such a case by simulating 20 spectra with 10 times longer exposures and with a reference model different from the basic one, described in Sec. 4.1. In this model all parameters are the same as in the basic one, only the disc line component is weaker, with equivalent width equal to the equivalent width of the Gaussian component, i.e., 60 eV. Using these data and those from basic simulations we have checked how the average depends on the relative share of different spectra in entire sample.

## 5 DISCUSSION

### 5.1 Best method

The best results are obtained for methods Ia, Ib and Ic applied to non-binned data, as presented in the bottom panel of Fig. 6. Only these methods almost perfectly reproduce the shape of the iron line on both its sides. There is a spread of results for higher energies, above 7 keV, but these discrepancies are symmetric and appear due to small statistics in this energy range. Methods Ia and Ib used for data binned up also work well, but here both red and blue wings of the line are slightly but systematically underestimated, as can

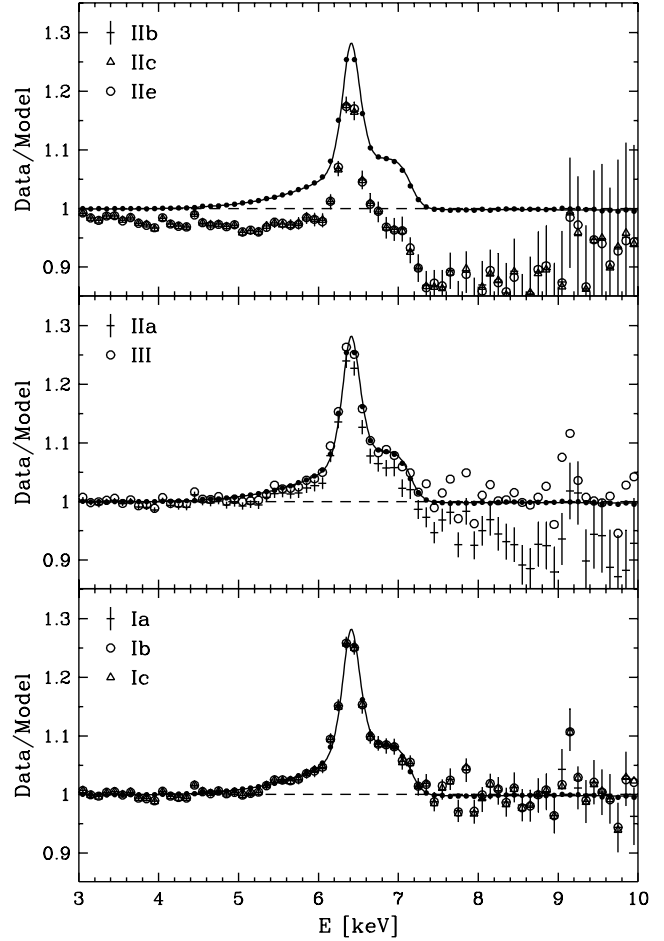


Figure 6. Averaging methods applied to data/model ratios obtained for non-binned spectra and continuum model fitted with C-statistic. Methods are denoted as in Table 1.

be seen from Fig. 7. For higher energies the spread of results is damped due to initial grouping of the input bins, however, owing to the same fact, spurious maxima are produced around 9.2 and 9.8 keV. Then, even with the best methods, averaging binned up data cannot be considered to be reliable for the higher energy boundary of ASCA SIS range. The third procedure from this group, method Ic, using bin weights  $b_i$ , fails for binned up spectra; this behaviour is explained in Sec. 5.2.

Methods based on averaging with the standard weights  $w_i$  (IIa-IIe) obviously cannot work properly for a continuum modelled with the C-statistic. This is clearly seen in the upper part of Figs. 6 and 7, where all these procedures fail completely to reproduce the continuum slope. For the same reason, methods using the probability functions do not work well for continuum fitted with the  $\chi^2$  statistic, this is illustrated in the lower part of Fig. 8.

The ‘standard’ method, IIE, applied to binned up data (Fig. 8), can be used as a crude approximation of the average shape. The red and blue wings of iron line are here more underestimated than is observed for methods Ia-Ic in Fig. 7. Also the line peak is not well reproduced and the distortions induced by binning up are present in the high energy end of the spectrum. Compared with method IIb, which uses



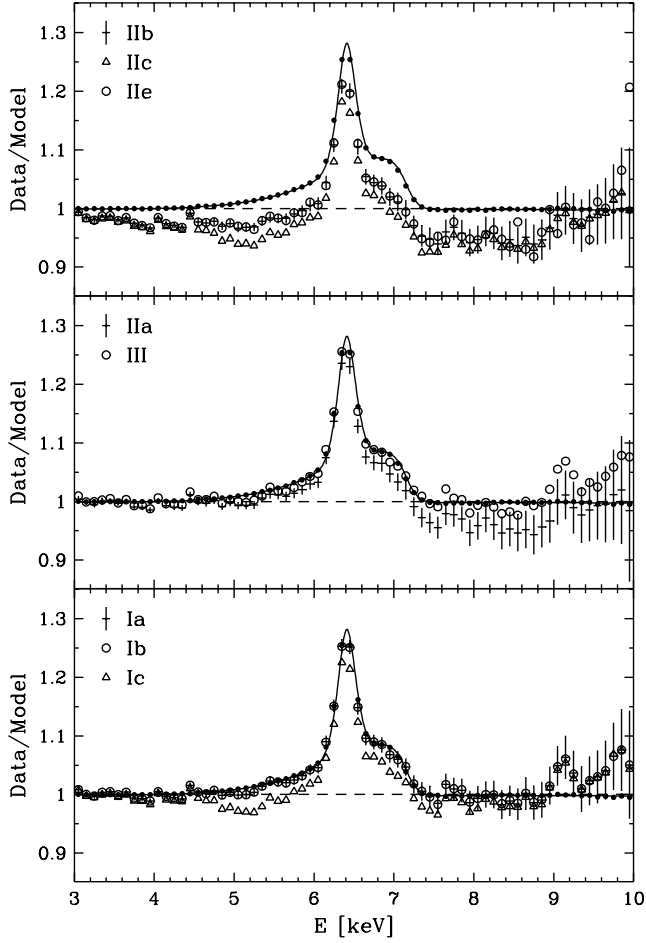


Figure 7. Averaging methods applied to data/model ratios obtained for binned up spectra and continuum model fitted with C-statistic.

all the input bins overlapping with the output bin (with  $g_i$  correction for boundary overlap), the 'standard' method results exhibit a larger spread for higher energies. This is simply the consequence of neglecting input bins with centres lying outside the output bin. Similarly to method Ic applied to binned up data (bottom part of Fig. 7), method IIc, using bin weights, produces a distorted shape for binned up input data (top panel of Figs. 7,8).

Results of two procedures based on prebinning, IIa and III, are shown in the middle panel of Figs. 6-8. Due to prebinning, method IIa is less sensitive to the improper accuracy weighting using  $w_i$  weights than all procedures averaging directly the input ratios (IIb-IIe). This effect is obviously stronger for single instrumental bins (Fig. 6), but appears clearly also for rebinned data (Fig. 7,8).

The arithmetic averaging with prebinning, method III, appears to work quite well for data obtained with the C-statistic, with, however, a larger spread of results observed for higher energies in the case of non-binned data (middle panel of Fig. 6). This spread illustrates the effect of neglecting any accuracy weights. The overall agreement between arithmetic and weighted averages (the proper ones, using the probability function) is understandable, due to the fact that the longest and the shortest exposure times used in

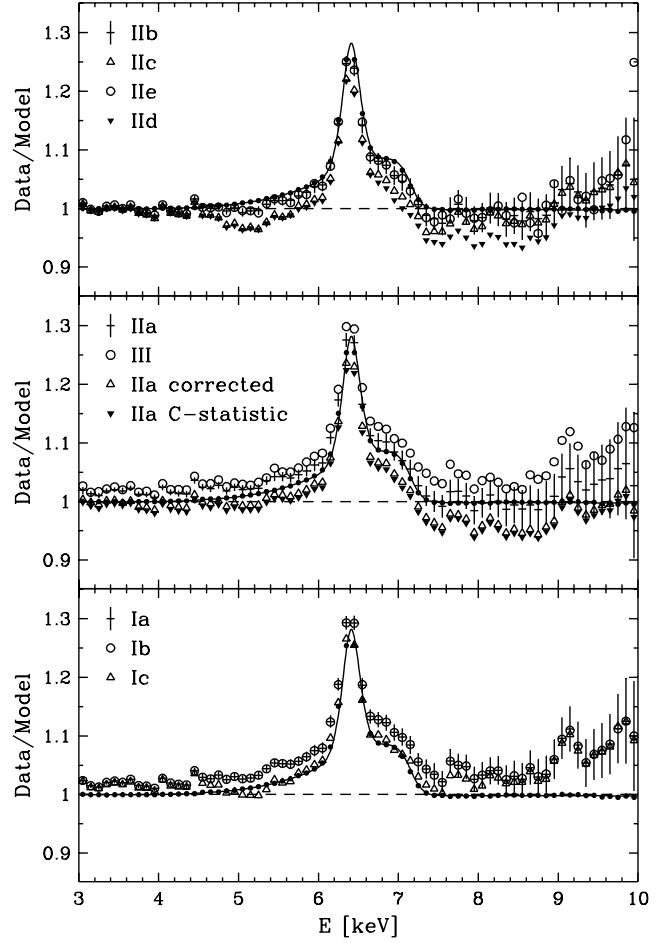


Figure 8. Averaging methods applied to data/model ratios obtained for binned up spectra and continuum model fitted with  $\chi^2$  statistic. Correction applied to the results of method IIa is explained in the text, see Sec. 5.1.

simulations differ only by factor of 2.5, thus the accuracy weights for different spectra also do not differ strongly.

The middle part of Fig. 8 shows that the method with prebinning and standard accuracy weights  $w_i$ , IIa, behaves quite differently from its counterpart without prebinning, method IIb (upper panel of this Figure). This can be explained by two effects. The first is an improper continuum model fitted with  $\chi^2$  statistics. Using the results presented in rows 3 and 5 of Table 2, we have corrected the average data/model ratios with a scaling function equal to the ratio of these mean power law models. The middle panel of Fig. 8 presents the results of this correction compared to the results of procedure IIa obtained for a continuum model fitted with C-statistic (i.e., the same as in the middle panel of Fig. 7). Now these results are in agreement and the rest of difference between methods IIb and IIa, applied to '2', input data, comes from the fact that the latter procedure is less affected by the imperfect accuracy weighting by widths  $w_i$ . This effect can be estimated from comparison between the results of methods IIb and IIa shown in the upper and middle panels, respectively, of Fig. 7.

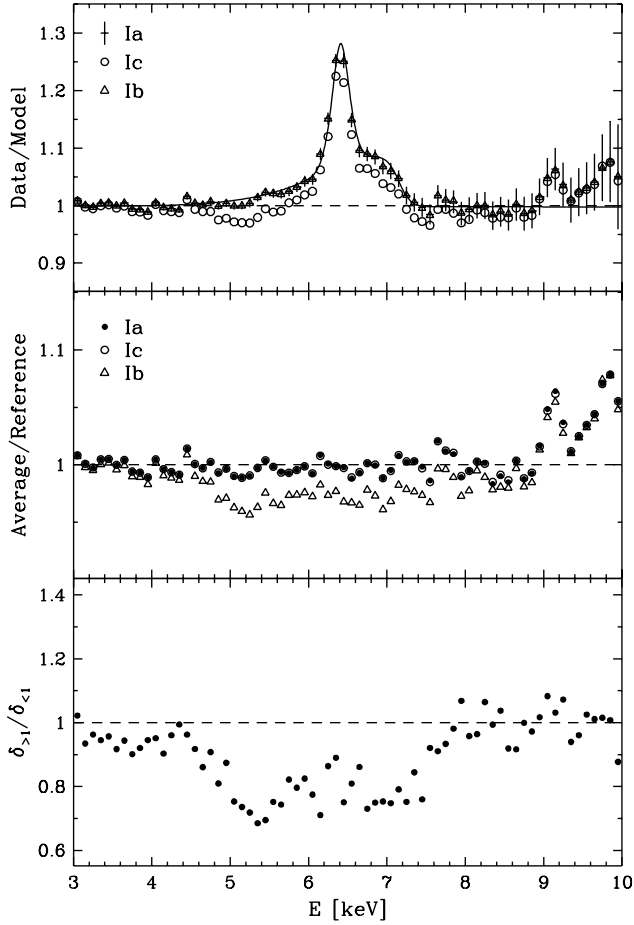


Figure 9. Test of averaging for biased (correlated) binning up. Upper panel: averaging results as in the lower panel of Fig. 7. Middle panel shows the ratios between these results and the reference shape. The ratios of arithmetic means of the overlap  $\delta$  for data/model ratios above and below 1 are presented in the bottom panel.

## 5.2 Biased vs. unbiased binning up

The average iron line shape for Sy1 nuclei, presented in Lubinski & Zdziarski (2001), was obtained with the procedure IId applied to initially binned up spectra. This is the standard manner used in X-ray spectral fitting with a  $\chi^2$  statistic to group single input bins to bins with at least 20 counts. As stated in Sec. 4.3, such a binning up is biased. However, it is hard to see how important this effect is in the situation where real data of unknown average shape are used. A quantitative estimate of the influence of this bias on the results of averaging can now be done, for data simulated using a known reference model.

In the upper panel of Fig. 9 the average spectral shapes obtained with methods Ia, Ib and Ic for binned up 'C-statistic' data are presented again as in Fig. 7. To show more clearly the differences between these methods, the ratios between their results and the reference average were plotted in the middle part of Fig. 9. The bottom panel of this Figure illustrates the ratio of the arithmetic averages of the input and output bins overlap,  $\delta$ , determined for data/model ratios above 1,  $\delta_{>1}$ , and below 1,  $\delta_{<1}$ . The deviation between

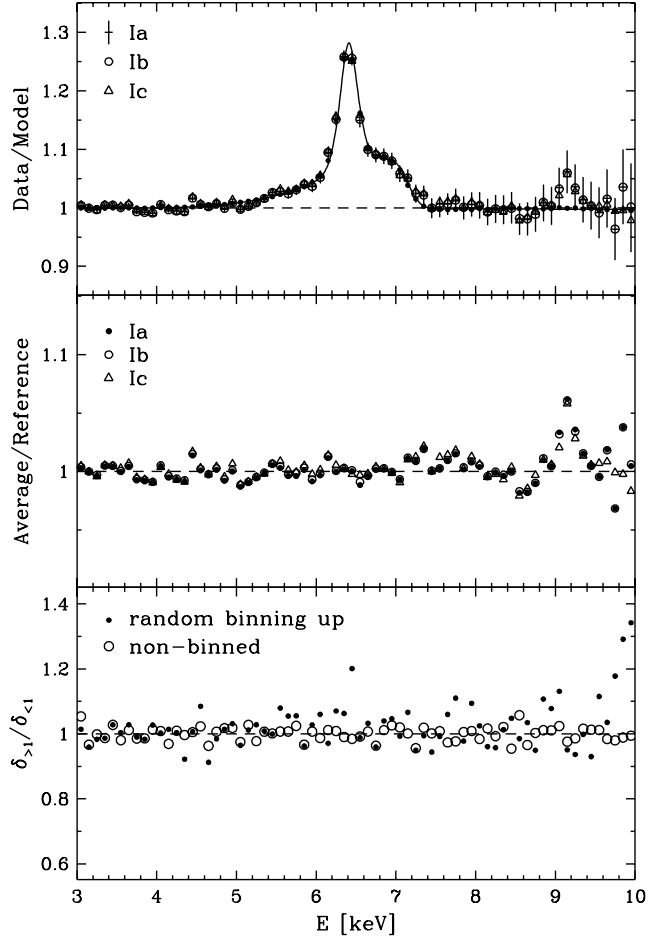


Figure 10. The same test as in Fig. 9 done for random (uncorrelated) binning up. Please note the change of the artificial features above 9 keV, in comparison with the results shown in Fig. 9, where different binning up pattern was applied.

the results of method using bin weights, Ib, and the reference results evidently follows the departure of  $\delta_{>1} = \delta_{<1}$  from unity. Fig. 10 presents the results of the same test applied to input data binned up with random binning, i.e., where the binning pattern for a given spectrum was taken from the other spectrum. Now all tested methods are in concordance, the procedure using bin weights reproduces the spectral shape equally well. The  $\delta_{>1} = \delta_{<1}$  ratios are close to unity, but with a larger spread than the same ratios obtained for non-binned data, shown for comparison in the bottom part of Fig. 10.

The results of method IId, i.e., that employed by Lubinski & Zdziarski (2001), are presented in the upper panel of Fig. 8. The correction introduced in Eq. (14) looks significant for higher energies ( $> 6$  keV), where  $g_1$  values are larger. However, as we have tested, the differences between the results of methods IId and IId disappear when these procedures are applied to the data binned up in non-biased way. Therefore, correction (14) manifests itself mainly by scaling the ratio errors to larger, proper values, almost not affecting the ratios themselves.

The scale of discrepancies between the results of procedures using bin weights (Ic, IId, IId), applied to the data

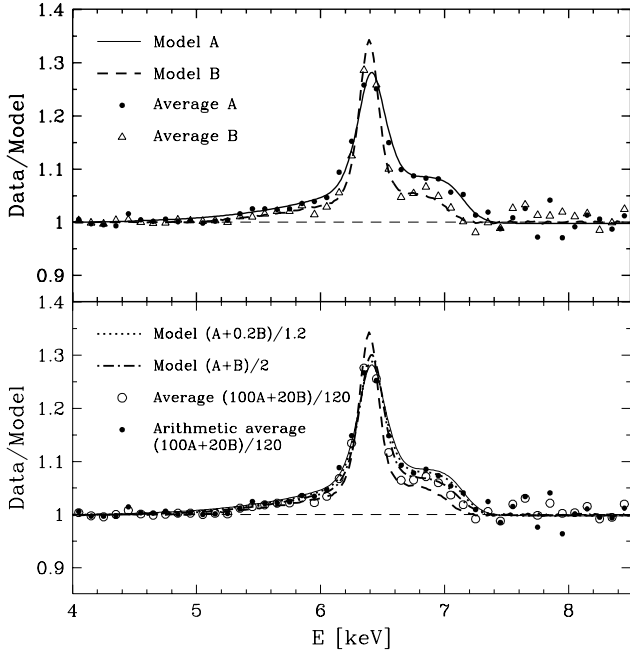


Figure 11. Test for sample with subsamples corresponding to two distinct spectral shapes. Upper panel shows the basic (A) and alternative (B) reference models together with averages obtained with method Ia for 100 basic (A) and 20 alternative (B) spectra. In the lower panel average reference models are presented, one with weights proportional to the number of spectra in given subsample, and second, with equal weights. The average for the entire sample of 120 spectra are performed with methods using the accuracy weights (Ia, circles) and without it (III, dots).

with biased binning up, and the reference results, shown in Figs. 7,8, seem to be large. Nevertheless, the spectra tested here are extremely weak, and the average spectral shape presented in Lubinski & Zdziarski (2001), obtained for better, on average, spectra of Sx1 nuclei, is only moderately affected by this mistake.

### 5.3 Inhomogeneous shapes

The results of averaging with method Ia applied to non-homogeneous input data are presented in Fig. 11. Two reference models are clearly distinct; the blue wings of the disc line component in these models are especially different. Assuming that the real composition of the studied objects is in proportion 1 to 0.2 to the advantage of the stronger disc line model, we should expect the mean to be closer to this model. However, we have assumed (see Sec. 4.4) that the objects with a weaker disc line component are about 10 times brighter than the rest of the sample. Then the weighted average (circles in the lower panel of Fig. 11) appears to be much closer to the shape of the brighter sources in comparison to the expected mean (dotted line in this Figure). This disadvantage can be removed with the use of arithmetic average, the results of which are shown with dots in the lower part of Fig. 11. As already mentioned in Sec. 5.1, arithmetic averaging leads to a larger spread in results, thus it is advisable to check the homogeneity of entire sample by dividing it to subsamples, grouped accidentally or according to some con-

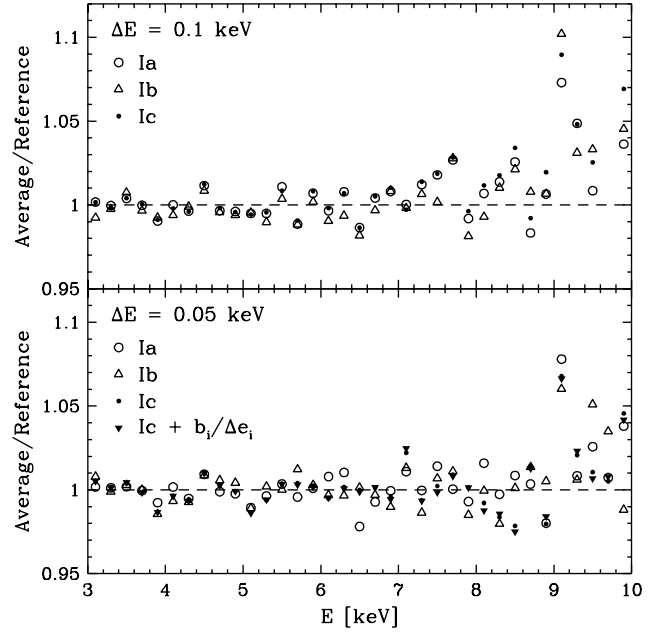


Figure 12. Averages with and without bin weights. Results of a given method are presented as the ratio between them and the results of the reference averaging. The upper panel shows the results for the output bin width equal to 0.1 keV, in the lower panel results for 0.05 keV output bins are presented. For clarity, results are grouped (arithmetically) to 0.2 keV bins.

dition. Afterwards, the weighted averages of approximately homogeneous subsamples can be averaged arithmetically.

In the case of Sx1 nuclei the spectra are known to be different for various objects in various spectral states and usually the values of their physical parameters are distributed over a wide range. However, there may exist samples of objects exhibiting clearly distinct physical character. Then the average over the entire sample will not describe any real object but, again, this can be easily checked by comparing the results for subsamples.

### 5.4 Incomplete information

The main reason of using bin weights  $b_i$  instead of prebinning in Lubinski & Zdziarski (2001) was the aim of having the possibility of studying all discrete spectral features in the average. There was also a second reason: there were many spectra, especially those observed with SIS1 spectrometer, which, due to the 'worse quality' tag, were truncated far below the upper instrumental limit (10 keV), at about 7 or 8 keV. In this case prebinning applied only to completely covered output bins leads to the loss of some information. To avoid this, one can treat input bins only partially covering the output bin as representative of the whole output bin, but now their share to the average is somewhat overestimated. On the contrary, usage of bin weights automatically reduces the significance of such incomplete information.

To better study the issue of incomplete information we have applied procedures with and without prebinning to the data, where half, chosen randomly, of the input bins was neglected in calculating the average. We have tested the best

methods, i.e., those based on the product of probability density functions, using the data with random binning up, since for the non-binned data the effect of bin weighting is reduced. The results of these tests are shown in Fig. 12, for two widths of the output bins, 0.1 and 0.05 keV. In the case of broader output bins there is no qualitative difference between the results of methods Ia and Ib, without bin weights, and method Ic, applying bin weights. For narrower output bins, in the region of Fe line peak (at 5.5–7 keV) the results of method Ic are more consistent with the reference average than the results of method Ib, whereas method Ia still does not seem to be clearly worse than method Ic. In general, bin weighting is advisable in the situation when one is going to study the most discrete features of the spectrum. However, for weak spectra the advantage of better resolution may not prevail over the benefit of higher accuracy coming from prebinning.

Application of more advanced bin weighting with additional  $b_i = e_i$  weights (see Sec. 2.1) is also shown in the lower part of Fig. 12, but it does not change the results significantly. Therefore, there is no need to apply complex bin weighting for data collected with instruments of rather limited spectral resolution.

The simultaneous fitting of many spectra, with the same line shape parameters but with different continuum models and line normalizations, can be considered as an alternative to fitting the spectrum obtained from the average shape. However, such an approach is inefficient in the case where there are more than a few dozen spectra. Handling a large set of input data and a much larger set of parameters associated with them is impractical for any fitting software due to time consuming computations and problems in assigning accuracy to the fitted values. On the other hand, the spectrum with the average shape can be easily fitted when the model incorporates some component describing the instrumental resolution, e.g., gaussian model in XSPEC.

## 6 CONCLUSIONS

We have studied the problem of averaging the spectral shapes in the case of weak X-ray spectra. The method applied in Lubinski & Zdziarski (2001) was substantially improved by more correct treatment of the Poisson character data and better modelling of the reference continuum. Various alternative approaches used to obtain the average spectral shape were tested with simulated data.

The reference average is correctly reproduced only by the methods based on the description of the data uncertainty by probability density functions (Eqs. 17–19). Among them, the method applying prebinning, i.e., summing the number of counts within the output bin (Eq. 18), is the simplest. Compared to the prebinning method, the procedure incorporating weights associated with the input and output bin overlap (Eq. 19) works better only in the case where the output bins are narrow and, accordingly, it is recommended for data taken with instruments of a very good spectral resolution.

There is no need to initially bin up the averaged data when the methods applying the probability functions are used and the continuum model is fitted with the C-statistic.

Only in this case is all of the information collected with the single, narrow channels of the instrument taken into account. Although the best methods also work well for spectra binned up in a non-biased way, the resulting spectral shape can be distorted due to the loss or mixing of information contained in single bins.

The usage of the  $\chi^2$  statistic in modelling of weak spectra leads to biased results and deformed average shape.

The arithmetic average used for prebinned data quite fairly reproduces the spectral shape, and can be recommended for approximately equally accurate input data or for testing the homogeneity of the averaged sample.

## ACKNOWLEDGMENTS

We would like to thank the referee for all comments and suggestions which helped to improve the presentation of our results. Discussions with Tomasz Bulik, Rafal Moderski and Grzegorz Wardzinski are warmly acknowledged. This research has been supported by grants from KBN (5P 03D 00821, 2P 03C 00619p1, 2).

## REFERENCES

- Amaud, K. A., 1996, in Jacoby G. H., Barnes J., eds. *ASP Conf. Ser. Vol. 101, Astronomical Data Analysis Software and Systems V*. Astron. Soc. Pac., San Francisco, p. 17
- Cash, W., 1979, *ApJ*, 228, 939
- Freeman, P. E., Doe, S., Siemiginowska, A., 2001, *SPIE Proceedings 4477*, November 2001, <http://cxc.harvard.edu/ciao/download/papers/mmissionindep.ps.gz>
- Freeman, P. E., 2001, *GSCF X-ray School*, <http://asc.harvard.edu/ciao/download/doc/freeman.pdf>
- Loader, C., 2000, *Fast and Accurate Computation of Binomial Probabilities*, <http://stat.cwru.edu/catherine/dbinom/dbinom.ps>
- Lored, T. J., 1992, in Feigelson E. D., Babu, G. J., eds. *Statistical Challenges in Modern Astronomy*, Springer-Verlag, New York, p. 275
- Lubinski, P., & Zdziarski, A. A., 2001, *MNRAS*, 323, L37
- Nandra, K., George, I. M., Mushotzky, R. F., Tumer, T. J., & Yaqoob, T., 1997, *ApJ*, 477, 602
- Nandra, K., George, I. M., Mushotzky, R. F., Tumer, T. J., & Yaqoob, T., 1997, *ApJ*, 488, L91
- Reeves, J., 2003, in Collin S., Combes F., Shlosman I., eds. *ASP Conf. Ser. Vol. 290, Active Galactic Nuclei: from Central Engine to Host Galaxy*, Astron. Soc. Pac., San Francisco, p. 35
- Reynolds, C. S., 1997, *MNRAS*, 286, 513
- Rolke, A. R., Lopez, A. M., 2001, *Nucl. Instr. & Meth. A* 458, 745
- Tanaka, Y., Nandra, K., Fabian, A. C., Inoue, H., Otani, C., Dotani, T., Hayashida, K., Iwasawa, K., Kii, T., Kunieda, H., Makino, F., & Matsuoka, M., 1995, *Nature*, 375, 659
- Yaqoob, T., Padmanabhan, U., Dotani, T., & Nandra, K., 2002, *ApJ*, 569, 487

## APPENDIX A: AVERAGE FLUX

Energy flux is defined as the ratio of the number of photons  $N_i$  collected in a given channel  $i$  and the product of the energy range of this channel  $e_i$ , exposure time  $T$  and effective (for the interesting energy range) area  $A$  of the instrument

$$hf_{i_i} = \frac{N_i}{AT e_i} \quad (A1)$$

Neglecting the relatively small errors of  $T$ ,  $e_i$  and  $A$  the accuracy of the flux is given by

$$hf_{i_i} = \frac{N_i}{AT e_i} \quad (A2)$$

In the case of no background, for Poisson distributed data,  $N_i$  is usually approximated by  $\bar{N}_i$ , hence the standard weighted average of fluxes measured for  $n_k$  input bins overlapping with the output bin has the form

$$\bar{f}_k = \frac{\sum_{i=1}^{X_k} \frac{(AT e_i)^2}{(N_i)^2} \frac{N_i}{AT e_i}}{\sum_{i=1}^{X_k} \frac{(AT e_i)^2}{(N_i)^2}} = \frac{AT \sum_{i=1}^{X_k} e_i}{(AT)^2 \sum_{i=1}^{X_k} \frac{(e_i)^2}{N_i}} \quad (A3)$$

Again using the equality  $N_i = hf_{i_i} e_i AT$  and inserting the output bin width  $E_k$  in the numerator and denominator we obtain

$$\bar{f}_k = \frac{\sum_{i=1}^{X_k} \frac{e_i}{E_k}}{\sum_{i=1}^{X_k} \frac{e_i}{E_k} \frac{1}{hf_{i_i}}} \quad (A4)$$

This is the harmonic mean, weighted with bin weights. In the situation where flux is approximately constant within the output bin, the factor  $1/hf_{i_i}$  can be taken out of the sum in denominator and we can insert  $hf_{i_i}$  in the sum in the numerator. Therefore, for the function of flux type, the weighted average given by (11) behaves in some sense similarly to the bin weighted average, Eq. (2).

The harmonic average is commonly recommended for the quantities of a relative character, defined as a ratio. Nevertheless, we cannot test this approach since for weak spectra the flux measured for narrow input bins is often equal to 0.

## APPENDIX B: POISSON DISTRIBUTION FOR UNKNOWN BACKGROUND

The X-ray background spectra are often weak and the background rate cannot be estimated with good accuracy. This uncertainty obviously affects the accuracy of the determined net source counts. There have been proposed solutions to this problem, modifying the Poisson distribution used to describe the source + background data. Below we compare the results of two of such methods with the distribution given by equation (15). The first procedure, classical (Rolke & Lopez 2001), is based on the likelihood ratios, the second, Bayesian (Loredo 1992), uses marginalization with respect to the background rate. For simplicity's sake, we assume here

that the source and background counts were taken during the same time and for the same size of the signal region.

Rolke & Lopez (2001) developed their method for setting confidence intervals for small signals in the presence of background. To find the confidence region they use the likelihood ratio test statistic in the form

$$l(\theta_0; x; y) = \frac{\max_{\theta} l(\theta; N; B) : \theta > 0}{\max_{\theta} l(\theta; N; B) : \theta > 0; \theta > 0} \quad (B1)$$

where  $\theta_0$  is the tested null hypothesis value of the net source counts. The likelihood function for source and background counts, given the observed  $N$  source counts and  $B$  background counts, is expressed as the product of two Poisson distributions

$$l(\theta; N; B) = \frac{(\theta + B)^N}{N!} e^{-(\theta + B)} \frac{B^B}{B!} e^{-B} \quad (B2)$$

As can be expected, the probability distribution derived from the likelihood ratio test is broader than the distribution obtained for the case of fixed background (Eq. (15)). This is the effect of calculating the likelihood function with variable  $B$ , what corresponds to taking the background uncertainty into account in this method.

The shape of the likelihood ratio  $l(\theta)$ , normalized to obtain maximal value equal to 1, is shown in Fig. B1. In the case, when the measured background is equal to 0, broadening affects the distribution only in the lowest, close to zero, region. (For  $B=0$  we have modified the Rolke & Lopez formula for maximizing the numerator in Eq. (B1), using the relation  $\max_{\theta} = \max_{\theta} (0; (N-2B)=2)$ .) The mode for this distribution is equal to  $N$ , as in the case of distribution obtained for the known background case. However, the mean for  $l(\theta)$  distribution is smaller or larger than  $N+1$ , depending on  $N$  and  $B$ .

The Bayesian method of inferring the signal strength in the situation of imprecisely measured background is presented in Loredo (1992). First we quote the formula for the posterior probability density derived by Loredo for the case when the background counts number is known

$$p(\theta; N; B) = C \frac{(\theta + B)^N e^{-(\theta + B)}}{N!} \quad (B3)$$

where the normalization constant  $C$  is equal to  $\sum_{i=0}^N \frac{B^i}{i!} e^{-B}$ . The mode for this distribution is equal to  $N$  and the mean,  $\bar{\theta}$ , equals to  $N+1$ .

For the unknown background case, the nuisance parameter, background rate  $B$ , is eliminated through marginalization, i.e., through integrating the integral of Eq. (B3) over  $B$ . The posterior probability distribution is calculated using the expansion of the binomial  $(\theta + B)^N$  and has the form

$$p(\theta; N; B) = \sum_{i=0}^{X_k} C_i \frac{\theta^i e^{-\theta}}{i!} \quad (B4)$$

with coefficients  $C_i$  given by formula

$$C_i = \sum_{j=0}^N \frac{2^j \frac{(N+B-j)!}{(N-j)!}}{2^j \frac{(N+B-j)!}{(N-j)!}} \quad (B5)$$

The above formula is interpreted in terms of a weighted average of the posterior densities calculated attributing 0,

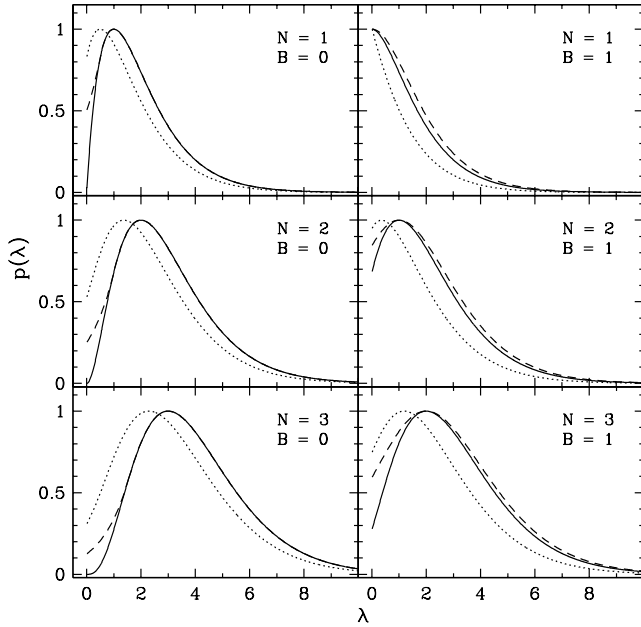


Figure B.1. Probability distributions for net source counts obtained with the use of different methods.  $N$  and  $B$  are the measured source and background counts, respectively. Solid line shows distribution obtained for the case, when the background rate is assumed to be known (Eq. (15)). Dashed line presents the distribution based on the likelihood ratio test, Eq. (B.1). Bayesian probability distribution, derived from the marginalization with respect to the background rate, Eq. (B.4), is plotted with the dotted line.

$1, \dots, N$  events to the signal. The  $C_i$  weights are the probabilities that  $i$  of the events observed on-source are from the source, provided that  $B$  counts are measured off-source.

The Bayesian probability distribution, computed from equation (B.4) and normalized to have maximum equal to 1, differs clearly from two other distributions shown in Fig. B.1. Its right tail is more extended but the major difference is the shift of its maximum towards lower values of  $\lambda$ . Depending on how  $N$  compares to  $B$ , this shift correlates inversely with the measured background counts, exceeding one unit for  $B = 0$  and approaching 0 for  $B = N$ . Using the relation  $\sum_{i=0}^N C_i = 1$  it is easy to show that the mean for the probability density given by (B.4) is equal to  $\sum_{i=0}^N C_i (i+1) = \sum_{i=0}^N C_i$ . Hence, taking into account the background uncertainty in the Bayesian procedure leads to lowering of the mean value, with the decrease depending on the measured background counts.

This paper has been typeset from a  $\text{\LaTeX}$  /  $\text{\LaTeX}$  file prepared by the author.